

Cavity-enhanced transport of charge

David Hagenmüller,¹ Johannes Schachenmayer,¹ Stefan Schütz,¹ Claudiu Genes,^{1,2} and Guido Pupillo¹

¹*IPCMS (UMR 7504) and ISIS (UMR 7006), University of Strasbourg and CNRS, 67000 Strasbourg, France*

²*Max Planck Institute for the Science of Light, Staudtstraße 2, D-91058 Erlangen, Germany*

(Dated: April 30, 2022)

We theoretically investigate charge transport through electronic bands of a mesoscopic one-dimensional system, where inter-band transitions are coupled to a confined cavity mode, initially prepared in its vacuum. This coupling leads to light-matter hybridization where the dressed fermionic bands interact via absorption and emission of dressed cavity-photons. Using a self-consistent non-equilibrium Green's function method, we compute electronic transmissions and cavity photon spectra and demonstrate how light-matter coupling can lead to a significant enhancement of charge conductivity in the steady-state. We find that depending on the ratio between cavity loss rate and electronic bandwidth, the system dynamics involves either a collective or an individual response of Bloch states, and explain how this affects the current enhancement.

PACS numbers: 05.60.Gg, 42.50.Pq, 74.40.Gh, 73.23.-b, 73.63.-b, 78.67.-n

The study of strong light-matter interactions [1–4] is playing an increasingly crucial role in understanding as well as engineering new states of matter with relevance to the fields of quantum optics [5–18], solid state physics [19–28], as well as quantum chemistry [29–33] and material science [34–50]. An emerging topic of interest is the modification of material properties using either external electro-magnetic radiation [51–53] or spatially confined modes such as in cavity quantum electrodynamics [54–59]. Recent experiments with organic semiconductors have demonstrated a dramatic enhancement of charge conductivity when molecules interact strongly with a surface plasmon mode initially prepared in its vacuum [60]. In principle, this can open up exciting new opportunities both for basic science and applications of organic electronics [61]. The microscopic mechanisms leading to charge conductivity enhancement, however, remain today largely unexplained. In this work, we propose a proof-of-principle model that features current enhancement due to the interaction with a confined bosonic mode in its ground state.

The setup we consider [see Fig. 1(a)] consists of a mesoscopic chain of N sites with two orbitals of energy ω_1 and ω_2 ($\hbar = 1$) in a 1D geometry, forming two bands in a tight-binding picture. The edges of the chain are connected to a source and a drain with a bias voltage across, respectively inserting and removing (spin-less) electrons at a rate Γ . The on-site interband transitions with energy $\omega_{21} = \omega_2 - \omega_1$ are resonantly coupled to a cavity mode with coupling strength g and loss rate κ . Electrons in the upper band are allowed to hop with a rate t , while no hopping is assumed in the lower band. Therefore, in the case $g = 0$ [Fig. 1(b)] electronic transmission can only arise due to the bare upper-band Bloch states. We find that for $g \neq 0$ [Fig. 1(c)], the two bands and the cavity photons hybridize to new states with enhanced transmission properties. Effectively, this results from a restoration of tunneling through the previously blocked

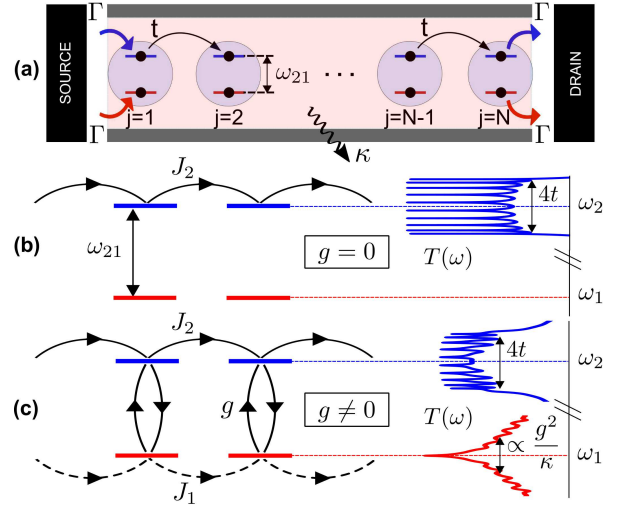


FIG. 1. (a) Model for 1D charge transport in the presence of a cavity. (b) In the absence of light-matter coupling, the hopping t allows for transmission in the upper band only. (c) In the presence of light-matter coupling (coupling strength g , photon loss rate κ), current can effectively flow through two dressed bands (the currents J_1 and J_2 are defined in the text) providing a new contribution of width $\propto g^2/\kappa$ in the transmission spectrum $T(\omega)$.

lower band, which in the best case can double the overall steady-state conductivity. In contrast to the usual Tavis-Cummings (TC) model for spins [62], where the system properties are determined by the ratio g/κ only, here, the nature of the light-matter coupling also crucially depends on the ratio $\kappa/4t$ between the cavity mode linewidth and the electronic bandwidth.

The steady-state current J can be computed through the electronic transmission spectrum $T(\omega)$ as

$$J = \frac{e\Gamma}{2} \int \frac{d\omega}{2\pi} T(\omega), \quad (1)$$

with ω the frequency and e the electron charge. The

dressing of the electronic bands and the cavity mode requires a self-consistent solution of the problem, which we obtain using a non-equilibrium Green's function method [63–72]. For $g \neq 0$, we show that $T(\omega)$ acquires a new additional transmission channel of width $\propto g^2/\kappa$, which is responsible for the current enhancement. This indicates that the latter is essentially driven by the individual coupling strength g . The final current results, however, from a competition of this individual dynamics with a coexisting collective electron-photon dynamics. The interplay between the two can be identified in the cavity photon spectrum and could be directly accessed in absorption spectroscopy experiments.

We consider the Hamiltonian $H_S = H_{\text{el}} + H_{\text{int}} + H_{\text{cav}}$, where

$$H_{\text{el}} = \sum_{j=1}^N \sum_{\alpha=1}^2 \omega_{\alpha} c_{\alpha,j}^{\dagger} c_{\alpha,j} - t \sum_{j=1}^{N-1} \left(c_{2,j+1}^{\dagger} c_{2,j} + \text{h.c.} \right) \quad (2)$$

$$H_{\text{int}} = g \sum_{j=1}^N \left(c_{2,j}^{\dagger} c_{1,j} a + c_{1,j}^{\dagger} c_{2,j} a^{\dagger} \right), \quad (3)$$

and $H_{\text{cav}} = \omega_{21} a^{\dagger} a$. Here, a is the bosonic annihilation operator for the cavity mode, while the fermionic operator $c_{\alpha,j}$ annihilates an electron in the orbital $\alpha = 1, 2$ on site j . The term H_{el} (2) is diagonalized in k -space as $H_{\text{el}} = \sum_{\alpha,k} \omega_{\alpha,k} \tilde{c}_{\alpha,k}^{\dagger} \tilde{c}_{\alpha,k}$, with $\omega_{2,k} = \omega_2 - 2t \cos(\pi k/(N+1))$ and $\omega_{1,k} = \omega_1$. The Hamiltonian H_S can be thus partitioned into a diagonal part $H_0 = H_{\text{el}} + H_{\text{cav}}$ with known eigenstates, and the light-matter interaction (3) which is treated perturbatively. In the following, all energies are in units of ω_{21} , which is set to 1. In the high-bias regime, i.e. when the Fermi level of the source (the drain) is higher (lower) than any other energy scale in the system, the transmission function entering Eq. (1) is derived as (see Supplemental Material [73])

$$T(\omega) = \text{Tr} \left[\underline{\sigma}^1 \circ \underline{A}_{\alpha}(\omega) + (\underline{\sigma}^N - \underline{\sigma}^1) \circ \Im \underline{G}_{\alpha}^{\leq}(\omega) \right]. \quad (4)$$

Here, $\text{Tr} \equiv \sum_{\alpha,k,k'}$, underlined quantities denote $N \times N$ matrices, \circ is the element-wise Hadamard product, \Im stands for imaginary part, and $\underline{\sigma}^j$ is a matrix of Fourier coefficients [73]. Equations (1) and (4) correspond to a generalization of the Landauer formula [74] to non-equilibrium mesoscopic systems [69, 73].

The first contribution of Eq. (4) involves the trace of the electron spectral function $\underline{A}_{\alpha}(\omega) = -2\Im \underline{G}_{\alpha}^r(\omega)$ in the band α . Here, $\underline{G}_{\alpha}^r(\omega)$ is the retarded Green function (GF) with matrix elements $G_{\alpha,k,k'}^r(\omega) = -i \int_0^{+\infty} d\tau e^{i\omega\tau} \langle \{ \tilde{c}_{\alpha,k}(\tau), \tilde{c}_{\alpha,k'}^{\dagger}(0) \} \rangle$, where $\langle \dots \rangle$ corresponds to the expectation value in the steady-state. Physically, the quantity $\sum_{k,k'} A_{\alpha,k,k'}(\omega)$ simply corresponds to the normalized electron density of states (DOS) in the band α .

As implied by the spectral function normalization $\int d\omega A_{\alpha,k,k'}(\omega) = 2\pi \delta_{k,k'}$, the effect of light-matter in-

teractions on the steady-state current is entirely determined by the second term in Eq. (4). This contribution is proportional to the trace of the “lesser” electron GF, with matrix elements $G_{\alpha,k,k'}^{\leq}(\omega) = i \int_{-\infty}^{+\infty} d\tau e^{i\omega\tau} \langle \tilde{c}_{\alpha,k'}^{\dagger}(0) \tilde{c}_{\alpha,k}(\tau) \rangle$. From there, one can compute expectation values $2\pi n_{\alpha,k,k'} = \int d\omega \Im G_{\alpha,k,k'}^{\leq}(\omega)$ as well as real space populations $n_{\alpha,j} = \langle c_{\alpha,j}^{\dagger} c_{\alpha,j} \rangle$ in the steady-state [70]. The “lesser” GFs $\underline{G}_{\alpha}^{\leq}(\omega)$ can be calculated through the Keldysh equation $\underline{G}_{\alpha}^{\leq}(\omega) = \underline{G}_{\alpha}^r(\omega) \underline{\Sigma}_{\alpha}^{\leq}(\omega) \underline{G}_{\alpha}^a(\omega)$, where the retarded and advanced GFs satisfy the Dyson equation $\underline{G}_{\alpha}^{\beta}(\omega) = [(\underline{G}_{\alpha}^{0\beta}(\omega))^{-1} - \underline{\Sigma}_{\alpha}^{\beta}(\omega)]^{-1}$ ($\beta = r, a$).

The non-interacting ($g = 0$) electron GFs $\underline{G}_{\alpha}^{0\beta}(\omega)$ are defined in [73], and exhibit matrix elements proportional to $\delta_{k,k'}$. In the framework of the self-consistent Born approximation [70] (SCBA), the electron lesser self-energy (SE) is given by [73]

$$\underline{\Sigma}_{\alpha}^{\leq}(\omega) = ig^2 (1 - \delta_{\alpha,\alpha'}) \int \frac{d\omega'}{2\pi} \underline{G}_{\alpha'}^{\leq}(\omega + \omega') D^>(\omega') + i\Gamma \underline{\sigma}^1, \quad (5)$$

where $D^>(\omega)$ denotes the “greater” photon GF. The first contribution of Eq. (5) represents the electron SE correction due to the light-matter coupling, stemming from the emission/absorption of cavity excitations (i.e. the poles of $D^>(\omega)$) when electrons undergo optical transitions between the two bands. The second term $\propto \Gamma$ is exact, and represents the broadening of electron states due to the coupling between the chain and the leads. It is worth mentioning that the validity domains of the SCBA and the rotating wave-approximation [75] [used in Eq. (3)] overlap in such a way that the SCBA would break down if one included counter rotating terms $\propto (c_{2,j}^{\dagger} c_{1,j} a^{\dagger} + \text{h.c.})$.

The “greater” photon GF is defined as $D^>(\omega) = -i \int_{-\infty}^{+\infty} d\tau e^{i\omega\tau} \langle A(0)A(\tau) \rangle$ with $A = a + a^{\dagger}$, and satisfies the Keldysh equation $D^>(\omega) = D^r(\omega) \Pi^>(\omega) D^a(\omega)$. In a similar way to electrons, the equation of motion for the retarded and advanced photon GFs can be put into the Dyson form $D^{\beta}(\omega) = [(D_0^{\beta}(\omega))^{-1} - \Pi^{\beta}(\omega)]^{-1}$, where D_0 denotes the non-interacting photon GFs and $\Pi(\omega)$ the photon SE. Furthermore, the retarded photon GF can be used to introduce the normalized cavity photon DOS as $A_c(\omega) = -2\Im D^r(\omega)$, which can be directly accessed experimentally by measuring the cavity absorption spectrum. In the SCBA, $\Pi^>(\omega)$ is given by [73]

$$\begin{aligned} \Pi^>(\omega) = & -ig^2 (1 - \delta_{\alpha,\alpha'}) \text{Tr} \int \frac{d\omega'}{2\pi} \underline{G}_{\alpha}^>(\omega + \omega') \underline{G}_{\alpha'}^{\leq}(\omega') \\ & - i\kappa\theta(\omega), \end{aligned} \quad (6)$$

where the product of the two electron GFs is a matrix multiplication, and θ is the Heaviside function. The first contribution can be identified with the polarization function associated with the transition dipole moments, and provides a dressing of the bare cavity photon GF D_0 .

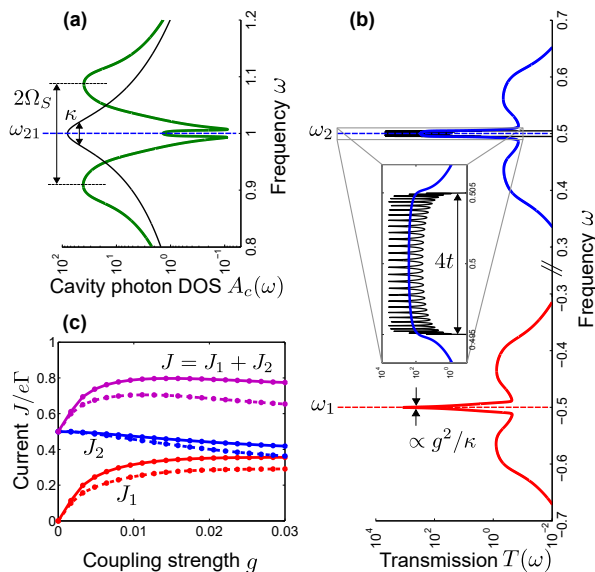


FIG. 2. Collective dressing regime, with $\Gamma = 2.5 \times 10^{-4}$, $t = 2.5 \times 10^{-3}$, and $\kappa = 0.05$. **(a)** (Log-scale) Cavity photon density of state $A_c(\omega)$ for $N = 30$. The thin black line corresponds to the bare cavity mode ($g = 0$), and the green line to the dressed one ($g = 0.03$). **(b)** (Log-scale) Transmission function $T(\omega)$ for $N = 30$. The thin black line corresponds to $g = 0$, while the red and blue lines correspond respectively to the vicinity of the lower ($\sim \omega_1 = -0.5$) and the upper band ($\sim \omega_2 = 0.5$) for $g = 0.03$. The central region is shown in the inset. **(c)** Current $J/(e\Gamma)$ versus coupling strength g for $N = 10$ (solid) and $N = 30$ (dashed). Red, blue, and magenta lines represent the partial currents J_1 , J_2 , and the total current J (see text).

The second contribution $\propto \kappa$ describes the cavity mode broadening due to photon losses, and is calculated exactly. Electron/photon SEs and GFs are thus related to each other by a self-consistent, closed set of integro-differential equations, that can be solved by iterations as explained in [73].

In the absence of light-matter coupling ($g = 0$), the steady-state current is entirely driven by the ratio t/Γ : it vanishes when $t \ll \Gamma$, and reaches its maximum $e\Gamma/2$ when $t \gg \Gamma$. In the latter regime, $T(\omega)$ consists of N well-resolved peaks of width $\propto \Gamma$ associated with the different Bloch states [63, 64, 67, 71, 76] [see Fig. 1(b)]. In the following, we focus on $t \gg \Gamma$ and $g \neq 0$.

In the presence of light-matter coupling, we find that the electron DOS is redistributed among the two bands, modifying the transmission spectrum. In particular, $T(\omega)$ acquires a peak of width $\propto g^2/\kappa$, centered around the bare lower band energy ω_1 . As shown in the Supplemental Material [73], this scaling can be explained by an analytical calculation up to second order in the perturbation (3). Here, we focus on the perturbative regime where $g^2/\kappa \lesssim 4t$ and $\kappa, g \ll \omega_{21}$. The steady-state current is now determined by the ratio $4t/\kappa$, allowing us to

distinguish between two main regimes in the following.

We denote the regime where $\kappa \gg 4t$ as “collective dressing regime”. This is depicted in Fig. 2 for an example with $N = 30$, $\Gamma = 2.5 \times 10^{-4}$, $t = 2.5 \times 10^{-3}$, and $\kappa = 0.05$. Figure 2(a) displays the steady-state cavity photon DOS, which is a key quantity to explore the interplay between charge transport and strong coupling physics. Here, for $g = 0$, the broad bare cavity mode of width κ (thin black line) is resonant to all transitions (with frequencies $\omega_{2,k} - \omega_1$) between the states of the lower flat band and the upper band Bloch states. The photon DOS in the coupled case with $g = 0.03$ is shown as a thick green line. The small peak centered at ω_{21} consists of $N - 1$ overlapping peaks (not resolved) with a small photon weight, which can be explained by an effective TC model [77]. In addition, the collective coupling to the cavity mode gives rise to two large polariton peaks separated by a splitting which we define as $2\Omega_S$.

The transmission spectrum $T(\omega)$ in the steady-state is shown in Fig. 2(b) for $g = 0$ (thin black line, Inset) and $g = 0.03$ (blue and red lines). We observe large peaks around each of the bare band energies ω_1 (red) and ω_2 (blue) that concentrate almost all of the spectral weight (note the log-scale). The key feature is the appearance of the large peak of width $\propto g^2/\kappa$ centered at the bare flat band energy ω_1 for $g \neq 0$. This peak originates from inter-band electronic transitions, concurrently with the absorption/emission of cavity photons with energy $\omega \approx \omega_{21}$ [small peak in Fig. 2(a)]. This new transmission channel corresponds to an effective hopping $\propto g^2/\kappa$ [see Fig. 1(c)], involving the individual coupling strength g and responsible for the observed current enhancement. In addition, the two polariton peaks from the cavity photon DOS give rise to small contributions outside the bandwidth $4t$, allowing for the injection of electrons at the energies $\sim \omega_{1,2} \pm \Omega_S$. However, they only contribute marginally to the overall transmission, because of their dominant photon-like character.

Figure 2(c) shows the effective currents J_1 and J_2 as a function of g , that are obtained by integrating $T(\omega)$ in the vicinity of ω_1 and ω_2 , respectively. The effective lower band current J_1 results from the new channel appearing around ω_1 and strongly increases in the considered range of g . The effective upper band current J_2 , in contrast, is found to decrease slightly, leading to a maximum in the overall current $J = J_1 + J_2$ [77]. We find that J decreases significantly when increasing the chain length N , which is an indication of the presence of collective effects (i.e. the relevant coupling parameter is Ω_S and not g , as explained in the following). When $\Omega_S \gg \kappa \gg 4t$, the photon DOS resembles more and more a Tavis-Cummings-like spectrum [62] with two well separated polariton peaks but no spectral weight at the bare transition frequency. Then, photonic excitations can not connect the two bands, thereby hampering band-dressing and the current enhancement. In the following, we will

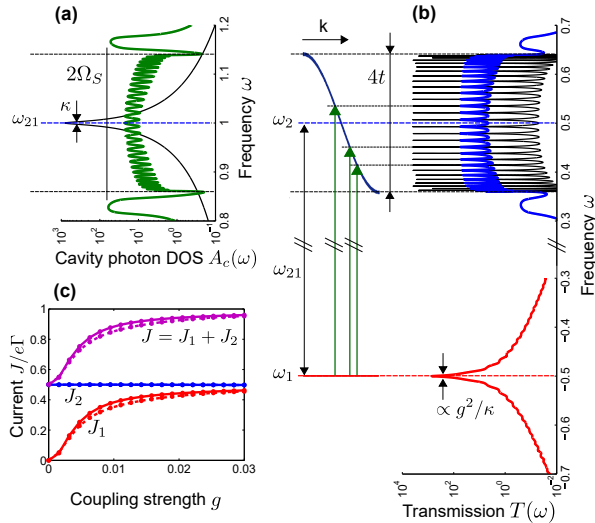


FIG. 3. Same quantities as in Fig. 2 in the individual dressing regime, with $\Gamma = 2.5 \times 10^{-4}$, $t = 0.07$, and $\kappa = 5 \times 10^{-3}$. N and g identical to Fig. 2. The Bloch states dispersion is plotted on the left side of panel (b), and a few interband transitions are depicted as vertical green arrows.

show that this collective effect can be largely circumvented when the cavity mode addresses only a few interband transitions.

We denote the regime where $\kappa \ll 4t$ as “individual dressing regime”. This situation is depicted in Fig. 3 for an example with $N = 30$, $\Gamma = 2.5 \times 10^{-4}$, $t = 0.07$, and $\kappa = 5 \times 10^{-3}$. Fig. 3(a) displays the cavity photon DOS for $g = 0.03$. In this regime, the narrow bare cavity mode (thin black line) is resonant with only a few inter-band transitions. Moreover, in this example, we are in a regime where both $g > \kappa$ and $g > \Delta\omega_k$, with $\Delta\omega_k \equiv \omega_{2,k+1} - \omega_{2,k}$ the energy spacing between two adjacent Bloch states. We find that once g is large enough to couple neighboring transitions together, two polariton peaks separated by a splitting $2\Omega_S$ begin to appear outside the electronic bandwidth. Inside the bandwidth, we now clearly resolve the $N - 1$ peaks with small photon weight.

The transmission spectrum $T(\omega)$ is shown in Fig. 3(b) for $g = 0$ (black line) and $g = 0.03$ (blue and red lines). Similarly as in the collective dressing regime, we observe a large peak of width $\propto g^2/\kappa$ centered at ω_1 , originating from inter-band electronic transitions with energy $\omega_{2,k} - \omega_1$ [$N - 1$ peaks in Fig. 3(a)]. Due to the reduced value of κ , this leads to a more pronounced current enhancement than before [Fig. 3(c)]. The effective upper band current J_2 is here almost independent of g . In total, the overall current enhancement is thus given by the effective lower band current J_1 , which strongly increases with g . In contrast to the collective dressing regime, J only slightly depends on the system size, showing that the individual dynamics largely dominates here.

Note that our two-band model exhibits a larger Hilbert

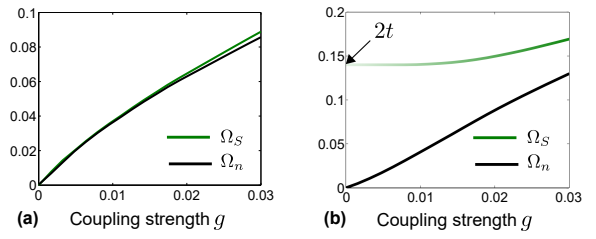


FIG. 4. Ω_S and Ω_n versus g for $N = 30$ and $\Gamma = 2.5 \times 10^{-4}$. (a) Collective dressing regime with $t = 2.5 \times 10^{-3}$ and $\kappa = 0.05$. (b) Individual dressing regime with $t = 0.07$ and $\kappa = 5 \times 10^{-3}$.

space (4^N) compared to the usual TC model for spins (2^N). The latter can be recovered only by constraining the electron number to one for each two-level system, providing a splitting $2g\sqrt{N}$ between the two polaritons. In contrast, in the collective dressing regime, our model exhibits a half-splitting Ω_S coinciding with the collective vacuum Rabi splitting $\Omega_n = g\sqrt{N_1 - N_2}$ ($N_\alpha = \sum_j n_{\alpha,j}$) [78], obtained from the steady-state population imbalance between the two bands [79]. Importantly, since sites with both orbitals occupied (or empty) are not effectively coupled to light, we always find $\Omega_n < g\sqrt{N}$, which implies that the TC model cannot be used to determine, e.g., the number of molecules based on measured Ω_S in experiments.

To further display the crossover between individual and collective regimes, we compare Ω_S to Ω_n , and summarize the results in Fig. 4. In the collective dressing regime [panel (a)], $\Omega_n \approx \Omega_S$, showing that the steady-state dynamics partly consists of collective oscillations of the charge density between the two bands with a frequency Ω_n , which reduce the current enhancement. In the individual dressing regime [panel (b)], Ω_S and Ω_n clearly differ, indicating that the individual dynamics with typical rate $\propto g^2/\kappa$, which is responsible for the current enhancement, largely dominates. Ω_S and Ω_n only get close to each other when $g \gtrsim 4t$, which results in recovering the physics of the collective dressing regime.

In this work, we introduced a proof-of-principle mechanism to enhance charge conductivity in a mesoscopic chain by coupling it to the vacuum field of a cavity. It is an exciting prospect to explore how this model can be extended to explain recent experiments with organic semiconductors, where order-of-magnitude enhancements in charge conductivity have been reported [60]. Possible extensions include coupling to multiple transmission channels in higher geometries, as well as the competition between light-matter coupling with Anderson localization in random lattices. In general, the method used in this article provides new perspectives for the investigation of many-body systems strongly coupled to cavity resonances or other bosonic (e.g. phononic) degrees of freedom.

Acknowledgements We are grateful to Thibault Chervy, Roberta Citro, Thomas Ebbesen, Cyriaque Genet, Emanuele Orgiu, and Paolo Samorì for inspiring discussions. Work in Strasbourg was supported by the ERC St-Grant ColDSIM (No. 307688), with additional funding from Rysq and ANR-FWF grant BLUESHIELD. C.G. benefited from financial support from the COST action NQO 1403 (Nano-scale Quantum Optics)

-
- [1] C. Weisbuch, M. Nishioka, A. Ishikawa, and Y. Arakawa, *Phys. Rev. Lett.* **69**, 3314 (1992).
- [2] D. G. Lidzey, D. D. C. Bradley, M. S. Skolnick, T. Virgili, S. Walker, and D. M. Whittaker, *Nature* **395**, 53 (1998).
- [3] J. M. Raimond, M. Brune, and S. Haroche, *Rev. Mod. Phys.* **73**, 565 (2001).
- [4] J. P. Reithmaier, G. Sek, A. Löffler, C. Hofmann, S. Kuhn, S. Reitzenstein, L. V. Keldysh, V. D. Kulakovskii, T. L. Reinecke, and A. Forchel, *Nature* **432**, 197 (2004).
- [5] T. Yoshie, A. Scherer, J. Hendrickson, G. Khitrova, H. M. Gibbs, G. Rupper, C. Ell, O. B. Shchekin, and D. G. Deppe, *Nature* **432**, 200 (2004).
- [6] S. Savasta, O. Di Stefano, V. Savona, and W. Langbein, *Phys. Rev. Lett.* **94**, 246401 (2005).
- [7] I. Fushman, D. Englund, A. Faraon, N. Stoltz, P. Petroff, and J. Vučković, *Science* **320**, 769 (2008).
- [8] S. I. Tsintzos, N. T. Pelekanos, G. Konstantinidis, Z. Hatzopoulos, and P. G. Savvidis, *Nature* **453**, 372 (2008).
- [9] K. G. Lagoudakis, M. Wouters, M. Richard, A. Baas, I. Carusotto, R. Andre, L. S. Dang, and B. Deveaud-Pledran, *Nat. Phys.* **4**, 706 (2008).
- [10] J. Claudon, J. Bleuse, N. S. Malik, M. Bazin, P. Jaffrennou, N. Gregersen, C. Sauvan, P. Lalanne, and J.-M. Gerard, *Nat. Photon.* **4**, 174 (2010).
- [11] S. Kena-Cohen and S. R. Forrest, *Nat. Photon.* **4**, 371 (2010).
- [12] P. Cristofolini, G. Christmann, S. I. Tsintzos, G. Deligeorgis, G. Konstantinidis, Z. Hatzopoulos, P. G. Savvidis, and J. J. Baumberg, *Science* **336**, 704 (2012).
- [13] F. Albert, K. Sivalertporn, J. Kasprzak, M. Strauß, C. Schneider, S. Höfling, M. Kamp, A. Forchel, S. Reitzenstein, E. A. Muljarov, and W. Langbein, *Nature Communications* **4**, 1747 (2013).
- [14] C. Schneider, A. Rahimi-Iman, N. Y. Kim, J. Fischer, I. G. Savenko, M. Amthor, M. Lermer, A. Wolf, L. Worschech, V. D. Kulakovskii, I. A. Shelykh, M. Kamp, S. Reitzenstein, A. Forchel, Y. Yamamoto, and S. Höfling, *Nature* **497**, 348 (2013).
- [15] R. Yalla, M. Sadgrove, K. P. Nayak, and K. Hakuta, *Phys. Rev. Lett.* **113**, 143601 (2014).
- [16] A. Goban, C.-L. Hung, J. D. Hood, S.-P. Yu, J. A. Muniz, O. Painter, and H. J. Kimble, *Phys. Rev. Lett.* **115**, 063601 (2015).
- [17] A. Javadi, I. Söllner, M. Arcari, S. L. Hansen, L. Midolo, S. Mahmoodian, G. Kiršanskė, T. Pregnolato, E. H. Lee, J. D. Song, S. Stobbe, and P. Lodahl, *Nature Communications* **6**, 8655 (2015).
- [18] A. Sipahigil, R. E. Evans, D. D. Sukachev, M. J. Burek, J. Borregaard, M. K. Bhaskar, C. T. Nguyen, J. L. Pacheco, H. A. Atikian, C. Meuwly, R. M. Camacho, F. Jelezko, E. Bielejec, H. Park, M. Lončar, and M. D. Lukin, *Science* **354**, 847 (2016).
- [19] A. Tredicucci, Y. Chen, V. Pellegrini, M. Börger, L. Sorba, F. Beltram, and F. Bassani, *Phys. Rev. Lett.* **75**, 3906 (1995).
- [20] J. Kasprzak, M. Richard, S. Kundermann, A. Baas, P. Jeambrun, J. M. J. Keeling, F. M. Marchetti, M. H. Szymanska, R. Andre, J. L. Staehli, V. Savona, P. B. Littlewood, B. Deveaud, and L. S. Dang, *Nature* **443**, 409 (2006).
- [21] K. Hennessy, A. Badolato, M. Winger, D. Gerace, M. Atatüre, S. Gulde, S. Falt, E. L. Hu, and A. Imamoglu, *Nature* **445**, 896 (2007).
- [22] A. Amo, D. Sanvitto, F. P. Laussy, D. Ballarini, E. d. Valle, M. D. Martin, A. Lemaître, J. Bloch, D. N. Krizhanovskii, M. S. Skolnick, C. Tejedor, and L. Vina, *Nature* **457**, 291 (2009).
- [23] H. Deng, H. Haug, and Y. Yamamoto, *Rev. Mod. Phys.* **82**, 1489 (2010).
- [24] I. Carusotto and C. Ciuti, *Rev. Mod. Phys.* **85**, 299 (2013).
- [25] J. M. Ménard, C. Poellmann, M. Porer, U. Leierseder, E. Galopin, A. Lemaître, A. Amo, J. Bloch, and R. Huber, *Nature Communications* **5**, 4648 (2014).
- [26] S. Smolka, W. Wuester, F. Haupt, S. Faelt, W. Wegscheider, and A. Imamoglu, *Science* **346**, 332 (2014).
- [27] O. Cotleț, S. Zeytinoglu, M. Sigrist, E. Demler, and A. Imamoglu, *Phys. Rev. B* **93**, 054510 (2016).
- [28] S. Zeytinoglu, A. Imamoglu, and S. Huber, “Engineering matter interactions using squeezed vacuum,” (2016), arXiv : 1608.02937v1 [cond-mat].
- [29] A. Shalabney, J. George, J. A. Hutchison, G. Pupillo, C. Genet, and T. W. Ebbesen, *Nature Communications* **6**, 5981 (2015).
- [30] J. George, A. Shalabney, J. A. Hutchison, C. Genet, and T. W. Ebbesen, *The Journal of Physical Chemistry Letters* **6**, 1027 (2015).
- [31] F. Herrera and F. C. Spano, *Phys. Rev. Lett.* **116**, 238301 (2016).
- [32] R. Chikkaraddy, B. de Nijs, F. Benz, S. J. Barrow, O. A. Scherman, E. Rosta, A. Demetriadou, P. Fox, O. Hess, and J. J. Baumberg, *Nature* **535**, 127 (2016).
- [33] J. Galego, F. J. Garcia-Vidal, and J. Feist, *Nature Communications* **7**, 13841 (2016).
- [34] A. Badolato, K. Hennessy, M. Atatüre, J. Dreiser, E. Hu, P. M. Petroff, and A. Imamoglu, *Science* **308**, 1158 (2005).
- [35] J. R. Tischler, M. S. Bradley, V. Bulović, J. H. Song, and A. Nurmikko, *Phys. Rev. Lett.* **95**, 036401 (2005).
- [36] A. V. Akimov, A. Mukherjee, C. L. Yu, D. E. Chang, A. S. Zibrov, P. R. Hemmer, H. Park, and M. D. Lukin, *Nature* **450**, 402 (2007).
- [37] L. Sapienza, A. Vasanelli, R. Colombelli, C. Ciuti, Y. Chassagneux, C. Manquest, U. Gennser, and C. Sirtori, *Phys. Rev. Lett.* **100**, 136806 (2008).
- [38] S. Aberra Guebrou, C. Symonds, E. Homeyer, J. C. Plenet, Y. N. Gartstein, V. M. Agranovich, and J. Bellessa, *Phys. Rev. Lett.* **108**, 066401 (2012).
- [39] P. Vasa, W. Wang, R. Pomraenke, M. Lammers, M. Maiuri, C. Manzoni, G. Cerullo, and C. Lienau, *Nat. Photon.* **7**, 128 (2013).
- [40] A. González-Tudela, P. A. Huidobro, L. Martín-Moreno, C. Tejedor, and F. J. García-Vidal, *Phys. Rev. Lett.*

- 110**, 126801 (2013).
- [41] D. Tanese, H. Flayac, D. Solnyshkov, A. Amo, A. Lemaître, E. Galopin, R. Braive, P. Senellart, I. Sagnes, G. Malpuech, and J. Bloch, *Nature Communications* **4**, 1749 (2013).
- [42] D. Ballarini, M. De Giorgi, E. Cancellieri, R. Houdré, E. Giacobino, R. Cingolani, A. Bramati, G. Gigli, and D. Sanvitto, *Nature Communications* **4**, 1778 (2013).
- [43] P. Bhattacharya, B. Xiao, A. Das, S. Bhowmick, and J. Heo, *Phys. Rev. Lett.* **110**, 206403 (2013).
- [44] J. D. Plumhof, T. Stöferle, L. Mai, U. Scherf, and R. F. Mahrt, *Nat. Mater.* **13**, 247 (2014).
- [45] L. Shi, T. K. Hakala, H. T. Rekola, J.-P. Martikainen, R. J. Moerland, and P. Törmä, *Phys. Rev. Lett.* **112**, 153002 (2014).
- [46] X. Liu, T. Galfsky, Z. Sun, F. Xia, E.-c. Lin, Y.-H. Lee, S. Kna-Cohen, and V. M. Menon, *Nat. Photon.* **9**, 30 (2015).
- [47] T. U. Tumkur, G. Zhu, and M. A. Noginov, *Optics Express* **24**, 3921 (2016).
- [48] J. A. Ówik, P. Kirton, S. De Liberato, and J. Keeling, *Phys. Rev. A* **93**, 033840 (2016).
- [49] M. D. LaCount and M. T. Lusk, *Physical Review A* **93**, 063811 (2016).
- [50] R. T. Grant, P. Michetti, A. J. Musser, P. Gregoire, T. Virgili, E. Vella, M. Cavazzini, K. Georgiou, F. Galeotti, C. Clark, J. Clark, C. Silva, and D. G. Lidzey, *Advanced Optical Materials* **4**, 16151623 (2016).
- [51] M. Mitrano, A. Cantaluppi, D. Nicoletti, S. Kaiser, A. Perucchi, S. Lupi, P. Di Pietro, D. Pontiroli, M. Ricc, S. R. Clark, D. Jaksch, and A. Cavalleri, *Nature* **530**, 461 (2016).
- [52] S. Masayuki, R. Kato, and H. M. Yamamoto, *Science* **347**, 743 (2015).
- [53] G. Mazza and A. Georges, “Non-equilibrium superconductivity in driven alkali-doped fullerides,” (2017), arXiv:1702.04675 [cond-mat.supr-con].
- [54] S. De Liberato and C. Ciuti, *Phys. Rev. B* **79**, 075317 (2009).
- [55] F. P. Laussy, A. V. Kavokin, and I. A. Shelykh, *Phys. Rev. Lett.* **104**, 106402 (2010).
- [56] S. Morina, O. V. Kibis, A. A. Pervishko, and I. A. Shelykh, *Phys. Rev. B* **91**, 155312 (2015).
- [57] J. Feist and F. J. Garcia-Vidal, *Phys. Rev. Lett.* **114**, 196402 (2015).
- [58] J. Schachenmayer, C. Genes, E. Tignone, and G. Pupillo, *Phys. Rev. Lett.* **114**, 196403 (2015).
- [59] A. Kavokin and P. Lagoudakis, *Nat. Mater.* **15**, 599 (2016).
- [60] E. Orgiu, J. George, J. Hutchison, E. Devaux, J. F. Dayen, B. Doudin, F. F. Stellacci, C. Genet, J. Schachenmayer, C. Genes, G. Pupillo, P. Samori, and T. W. Ebbesen, *Nature Materials* **14**, 1123 (2015).
- [61] A. Salleo, *Nat. Mater.* **14**, 1077 (2015).
- [62] M. Tavis and F. W. Cummings, *Phys. Rev.* **170**, 379 (1968).
- [63] C. Caroli, R. Combescot, P. Nozieres, and D. Saint-James, *Journal of Physics C: Solid State Physics* **4**, 916 (1971).
- [64] C. Caroli, R. Combescot, P. Nozieres, and D. Saint-James, *Journal of Physics C: Solid State Physics* **5**, 21 (1972).
- [65] J. L. D’Amato and H. M. Pastawski, *Phys. Rev. B* **41**, 7411 (1990).
- [66] S. Datta, *Electronic Transport in Mesoscopic Systems:* (Cambridge University Press, Cambridge, 1995).
- [67] T.-S. Kim and S. Hershfield, *Phys. Rev. B* **65**, 214526 (2002).
- [68] D. Roy and A. Dhar, *Phys. Rev. B* **75**, 195110 (2007).
- [69] H. Haug and A.-P. Jauho, *Quantum Kinetics in Transport and Optics of Semiconductors* (Springer-Verlag Berlin Heidelberg, 2008).
- [70] M. Pourfath, *The Non-Equilibrium Green’s Function Method for Nanoscale Device Simulation* (Springer-Verlag Wien, 2014).
- [71] R. J. Doornenbal, G. Skantzaris, and H. T. C. Stoof, *Phys. Rev. B* **91**, 045419 (2015).
- [72] D. Gruss, K. A. Velizhanin, and M. Zwolak, *Scientific Reports* **6**, 24514 (2016).
- [73] D. Hagenmüller, J. Schachenmayer, S. Schütz, C. Genes, and G. Pupillo, Supplemental Material for “Cavity-enhanced transport of charge” (2017).
- [74] R. Landauer, *Zeitschrift für Physik B Condensed Matter* **68**, 217 (1987).
- [75] M. O. Scully and M. S. Zubairy, *Quantum Optics:* (Cambridge University Press, Cambridge, 1997).
- [76] A. Dhar, K. Saito, and P. Hänggi, *Phys. Rev. E* **85**, 011126 (2012).
- [77] Note that the overall current can be also obtained using a master equation approach as we detail in [73]. We find that the results are consistent with the non-equilibrium Green’s function method.
- [78] Y. Todorov, A. M. Andrews, R. Colombelli, S. De Liberato, C. Ciuti, P. Klang, G. Strasser, and C. Sirtori, *Phys. Rev. Lett.* **105**, 196402 (2010).
- [79] The qualitative features of the cavity photon DOS of Figs. 2(a) and 3(a) follow from a simple generalization of the TC Hamiltonian [62]: $H_{TC} = \omega_0 a^\dagger a + \sum_{k=1}^N (\omega_{2,k} - \omega_1) \sigma_k^z / 2 + g \sum_k (\sigma_k^+ a + \sigma_k^- a^\dagger)$, where σ_k^z, σ_k^\pm are the Pauli operators associated with the N inter-band transitions.
- [80] S. Engelsberg and J. R. Schrieffer, *Phys. Rev.* **131**, 993 (1963).

SUPPLEMENTAL MATERIAL

Steady-state current and Green's functions

In this section, we present the non-equilibrium Green's function (NEGF) method, based on a generalization of the model presented in the Chapter 12 of Ref. [69]. In the following, we will consider $\hbar = 1$, and use the short-hand notations $\partial_\tau \equiv \frac{\partial}{\partial \tau}$ and $\delta_{f(\tau)} \equiv \frac{\delta}{\delta f(\tau)}$, for function and functional derivatives respectively. The coupling of the atom chain to the leads can be described by the tunnelling Hamiltonian:

$$H_T = \sum_{\alpha} \sum_{\eta=s,d} \sum_{\mathbf{q}} \omega_{\mathbf{q}} b_{\alpha,\mathbf{q},\eta}^{\dagger} b_{\alpha,\mathbf{q},\eta} + \sum_{\alpha} \sum_{\eta=s,d} \sum_{j,\mathbf{q}} \lambda_{j,\mathbf{q},\eta} \left(c_{\alpha,j} b_{\alpha,\mathbf{q},\eta}^{\dagger} + b_{\alpha,\mathbf{q},\eta} c_{\alpha,j}^{\dagger} \right), \quad (7)$$

with coupling constants $\lambda_{j,\mathbf{q},s} = \lambda_{\mathbf{q}}$ for $j = 1$, $\lambda_{j,\mathbf{q},s} = 0$ for $j \neq 1$, and $\lambda_{j,\mathbf{q},d} = \lambda_{\mathbf{q}}$ for $j = N$, $\lambda_{j,\mathbf{q},d} = 0$ for $j \neq N$. The operators $b_{\alpha,\mathbf{q},\eta}^{\dagger}$ ($b_{\alpha,\mathbf{q},\eta}$) create (annihilate) a fermion in the state (α, \mathbf{q}) of the lead η , and obey fermionic commutation relations. \mathbf{q} is a continuous index interpreted as the 2d electron wavevector in the leads. The cavity mode with energy ω_0 is coupled to a photonic bath described by the 3d mode continuum with wavevectors \mathbf{p} . The corresponding Hamiltonian is written in terms of the extra-cavity photon operators $a_{\mathbf{p}}^{\dagger}$ and $a_{\mathbf{p}}$ (obeying bosonic commutation rules) as:

$$H_{\text{ph}} = \sum_{\mathbf{p}} \omega_{\mathbf{p}} a_{\mathbf{p}}^{\dagger} a_{\mathbf{p}} + \sum_{\mathbf{p}} \mu_{\mathbf{p}} A_{\mathbf{p}} A, \quad (8)$$

where $A_{\mathbf{p}} = a_{\mathbf{p}} + a_{\mathbf{p}}^{\dagger}$. Using Fourier series of the chain operators $c_{\alpha,j} = \sum_{k=1}^N \varphi_k^j \tilde{c}_{\alpha,k}$, with $\varphi_k^j = \sqrt{2/(N+1)} \sin(\pi j k / (N+1))$, the total (system+reservoirs) Hamiltonian $H = H_S + H_{\text{ph}} + H_T$ can be written in k -space. Formally including the counter-rotating terms in the coupling Hamiltonian H_{int} in Eq. (3) of the main text, we get:

$$\begin{aligned} H_S &= \sum_{\alpha,k} \omega_{\alpha,k} \tilde{c}_{\alpha,k}^{\dagger} \tilde{c}_{\alpha,k} + \omega_0 a^{\dagger} a + g \sum_k \left(\tilde{c}_{2,k}^{\dagger} \tilde{c}_{1,k} + \tilde{c}_{1,k}^{\dagger} \tilde{c}_{2,k} \right) A \\ H_T &= \sum_{\alpha} \sum_{\eta,\mathbf{q}} \omega_{\mathbf{q}} b_{\alpha,\mathbf{q},\eta}^{\dagger} b_{\alpha,\mathbf{q},\eta} + \sum_{\eta,\mathbf{q}} \sum_{\alpha,k} \lambda_{\mathbf{q}} \varphi_k^{j_{\eta}} \left(\tilde{c}_{\alpha,k} b_{\alpha,\mathbf{q},\eta}^{\dagger} + b_{\alpha,\mathbf{q},\eta} \tilde{c}_{\alpha,k}^{\dagger} \right), \end{aligned} \quad (9)$$

where $\omega_{2,k} = \omega_2 - 2t \cos(\pi k / (N+1))$, $\omega_{1,k} = \omega_1 \forall k$, $j_s = 1$ and $j_d = N$. In the steady-state, the charge current J_{η} flowing through the lead η is such that $J_s = -J_d$, and is given by $J_{\eta} = -e \partial_t \langle N_{\eta} \rangle = -ie \langle [H, N_{\eta}] \rangle$, where $\langle \dots \rangle$ stands for quantum average in the ground state of the total Hamiltonian H , and $N_{\eta} = \sum_{\alpha,\mathbf{q}} b_{\alpha,\mathbf{q},\eta}^{\dagger} b_{\alpha,\mathbf{q},\eta}$ is the number of electrons in the lead η . A direct calculation of the commutator allows us to first express the current in terms of a Green's function (GF) which describes the correlations between the leads and the atom chain:

$$J_{\eta} = -2e \sum_{\alpha,k} \sum_{\mathbf{q}} \varphi_k^{j_{\eta}} \lambda_{\mathbf{q}} \int \frac{d\omega}{2\pi} \Re \left[G_{\alpha,k,\mathbf{q},\eta}^{<}(\omega) \right] \quad (10)$$

where \Re stands for real part, and $G_{\alpha,k,\mathbf{q},\eta}^{<}(\omega) = i \int d(\tau - \tau') e^{i\omega(\tau - \tau')} \langle b_{\alpha,\mathbf{q},\eta}^{\dagger}(\tau') \tilde{c}_{\alpha,k}(\tau) \rangle$. Introducing the time-ordered mixed system-leads GF $G_{\alpha,k,\mathbf{q},\eta}(\tau) = -i \langle \mathcal{T} \tilde{c}_{\alpha,k}(\tau) b_{\alpha,\mathbf{q},\eta}^{\dagger}(\tau') \rangle$, where the time-ordered product is defined as $\mathcal{T} A(\tau) B(\tau') = \Theta(\tau - \tau') A(\tau) B(\tau') - \Theta(\tau' - \tau) B(\tau') A(\tau)$, the equation of motion satisfied by $G_{\alpha,k,\mathbf{q},\eta}$ can be found by taking the time derivative $\partial_{\tau'} G_{\alpha,k,\mathbf{q},\eta}(\tau - \tau')$, and then calculate the different commutators originating from the Heisenberg equation $\partial_{\tau'} b_{\alpha,\mathbf{q},\eta}^{\dagger}(\tau') = i [H, b_{\alpha,\mathbf{q},\eta}^{\dagger}](\tau')$:

$$\left(-i \frac{\partial}{\partial \tau'} - \omega_{\mathbf{q}} \right) G_{\alpha,k,\mathbf{q},\eta}(\tau - \tau') = -\lambda_{\mathbf{q}} \sum_{k'} \varphi_{k'}^{j_{\eta}} G_{\alpha,k,k'}(\tau - \tau'). \quad (11)$$

This equation of motion is then solved as:

$$G_{\alpha,k,\mathbf{q},\eta}(\omega) = -\lambda_{\mathbf{q}} \sum_{k'} G_{\alpha,k,k'}(\omega) \mathcal{G}_{\mathbf{q},\eta}(\omega), \quad (12)$$

where $G_{\alpha,k,k'}(\omega) = -i \int d(\tau - \tau') e^{i\omega(\tau - \tau')} \langle \mathcal{T} \tilde{c}_{\alpha,k}(\tau) \tilde{c}_{\alpha,k'}^\dagger(\tau') \rangle$ denotes the time-ordered GF of the atom chain, and the leads time-ordered GFs are defined as $\mathcal{G}_{\mathbf{q},\eta}(\omega) = -i \int d(\tau - \tau') e^{i\omega(\tau - \tau')} \langle \mathcal{T} b_{\alpha,\mathbf{q},\eta}(\tau) b_{\alpha,\mathbf{q},\eta}^\dagger(\tau') \rangle_0 = 1/(\omega - \omega_{\mathbf{q}})$. Here, $\langle \cdots \rangle_0$ refers to the expectation value in the ground state of the lead Hamiltonian $\sum_{\alpha,\eta,\mathbf{q}} \omega_{\mathbf{q}} b_{\alpha,\mathbf{q},\eta}^\dagger b_{\alpha,\mathbf{q},\eta}$. We now use the Langreth rules [69] on Eq. (12), and get:

$$G_{\alpha,k,\mathbf{q},\eta}^<(\omega) = -\lambda_{\mathbf{q}} \sum_{k'} \left(G_{\alpha,k,k'}^r(\omega) \mathcal{G}_{\mathbf{q},\eta}^<(\omega) + G_{\alpha,k,k'}^<(\omega) \mathcal{G}_{\mathbf{q},\eta}^a(\omega) \right), \quad (13)$$

where r and a stand for retarded and advanced GFs respectively. Converting the summation over \mathbf{q} in Eq. (10) into a frequency integral $\sum_{\mathbf{q}} \rightarrow \int_0^\infty d\omega \rho(\omega)$, where $\rho(\omega)$ represents the electron density of states in the leads, we introduce the tunnelling rate between the atom chain and the leads as $\Gamma(\omega) = 2\pi\rho(\omega)\lambda^2(\omega)$. For sake of simplicity, we ignore the energy dependence of the tunnelling rate ($\Gamma(\omega) \equiv \Gamma$), which amounts to neglect the non-local temporal response (Markovian leads). Finally, using the results:

$$\mathcal{G}_{\mathbf{q},\eta}^<(\omega) = 2i\pi\delta(\omega - \omega_{\mathbf{q}})n_\eta(\omega) \quad \text{and} \quad \mathcal{G}_{\mathbf{q},\eta}^a(\omega) = \frac{1}{\omega - \omega_{\mathbf{q}} - i0^+}, \quad (14)$$

where $n_\eta(\omega)$ is the Fermi occupation number of the lead η , and 0^+ an infinitesimal positive quantity, Eq. (10) takes the form given by Eqs. (1) and (4) in the main text.

Electron Green's functions

Let us demonstrate that the electron GFs in the atom chain satisfy a Dyson equation of motion. As before, we first calculate the time derivative $\partial_\tau G_{\alpha,k,k'}(\tau - \tau')$ combined with the Heisenberg equation $\partial_\tau \tilde{c}_{\alpha,k}(\tau) = i[H, \tilde{c}_{\alpha,k}](\tau)$, and obtain:

$$(i\partial_\tau - \omega_{\alpha,k}) G_{\alpha,k,k'}(\tau - \tau') = \delta_{k,k'} \delta(\tau - \tau') + g(1 - \delta_{\alpha,\alpha'}) F_{\alpha',k,\alpha,k'}(\tau - \tau') - \sum_{\mathbf{q},\eta} \lambda_{\mathbf{q}} \varphi_k^{j\eta} G_{\mathbf{q},\eta,\alpha,k'}(\tau - \tau'), \quad (15)$$

where $G_{\mathbf{q},\eta,\alpha,k}(\tau - \tau') = -i \langle \mathcal{T} b_{\alpha,\mathbf{q},\eta}(\tau) \tilde{c}_{\alpha,k}^\dagger(\tau') \rangle$ is a mixed system-leads GF, and $F_{\alpha',k,\alpha,k'}(\tau - \tau') = -i \langle \mathcal{T} \tilde{c}_{\alpha',k}(\tau) \tilde{c}_{\alpha,k'}^\dagger(\tau') A(\tau) \rangle$ corresponds to a higher-order correlation function mixing the electronic and photonic degrees of freedom. The equation of motion for $G_{\mathbf{q},\eta,\alpha,k}$ can be derived similarly as in the previous section, providing:

$$G_{\mathbf{q},\eta,\alpha,k'}(\omega) = -\lambda_{\mathbf{q}} \sum_{k_1} \varphi_{k_1}^{j\eta} \mathcal{G}_{\mathbf{q},\eta}(\omega) G_{\alpha,k_1,k'}(\omega). \quad (16)$$

Following the procedure of Ref. [80], the correlation function $F_{\alpha',k,\alpha,k'}(\tau - \tau')$ can now be written in terms of GFs, by adding a vanishing source term $H' = \mathcal{J}A$ to the Hamiltonian H , and then taking the functional derivative $\delta_{\mathcal{J}(\tau)} G_{\alpha',k,\alpha,k'}(\tau - \tau')$, with:

$$G_{\alpha',k,\alpha,k'}(\tau - \tau') = -i \frac{\langle \mathcal{T} \tilde{c}_{\alpha',k}(\tau) \tilde{c}_{\alpha,k'}(\tau') e^{-i \int d\tau_1 H(\tau_1)} \rangle_0}{\langle e^{-i \int d\tau_1 H(\tau_1)} \rangle_0}. \quad (17)$$

The operation $\langle \cdots \rangle_0$ stands for quantum average in the ground state of the non-interacting Hamiltonian H_0 defined in the main text. After some manipulations using the functional derivative properties, we obtain:

$$F_{\alpha',k,\alpha,k'}(\tau - \tau') = ig \sum_{k_1,k_2} \int d\tau_1 \int d\tau_2 \int d\tau_3 G_{\alpha',k,k_1}(\tau - \tau_1) \Lambda_{\alpha',k_1,\alpha,k_2}(\tau_1, \tau_2, \tau_3) D(\tau_3 - \tau) G_{\alpha,k_2,k'}(\tau_2 - \tau'), \quad (18)$$

where the time-ordered photon Green function is defined as $D(\tau_3 - \tau) = \delta_{\mathcal{J}(\tau)} \langle A(\tau_3) \rangle = -i \langle \mathcal{T} A(\tau_3) A(\tau) \rangle$, and the so-called vertex function $\Lambda_{\alpha',k_1,\alpha,k_2}(\tau_1, \tau_2, \tau_3) = -\frac{1}{g} \delta_{\langle A(\tau_3) \rangle} G_{\alpha',k_1,\alpha,k_2}^{-1}(\tau_1 - \tau_2)$. It can be shown that this vertex function satisfies a self-consistent equation[80] of the kind:

$$\Lambda_{\alpha',k_1,\alpha,k_2}(\tau_1, \tau_2, \tau_3) = (1 - \delta_{\alpha',\alpha}) \delta_{k_1,k_2} \delta(\tau_1 - \tau_2) \delta(\tau_1 - \tau_3) + \mathcal{O}(\Lambda^2), \quad (19)$$

where $\mathcal{O}(\Lambda^2)$ denotes a second order functional in Λ , providing vertex corrections[80] (crossed diagrams). In the full Born approximation (FBA), vertex corrections are neglected and we keep only the first term in the right-hand side of Eq. (19). Back to Eq. (15), we convert the summation over \mathbf{q} into a frequency integral (see Sec.), and then use Eqs. (16), (18), and (19). Equation (15) finally takes a Dyson form in the frequency domain:

$$\sum_{k_1} ((G_{\alpha,k,k_1}^0(\omega))^{-1} - \Sigma_{\alpha,k,k_1}(\omega)) G_{\alpha,k_1,k'}(\omega) = \delta_{k,k'}, \quad (20)$$

with the FBA self-energy (SE):

$$\Sigma_{\alpha,k,k'}(\omega) = ig^2 (1 - \delta_{\alpha_1,\alpha}) \int \frac{d\omega'}{2\pi} G_{\alpha_1,k,k'}(\omega + \omega') D(\omega') + \sum_{\mathbf{q},\eta} \lambda_{\mathbf{q}}^2 \varphi_k^{j\eta} \varphi_{k'}^{j\eta} \mathcal{G}_{\mathbf{q},\eta}(\omega), \quad (21)$$

and the non-interacting GF $G_{\alpha,k,k_1}^0(\omega) = \delta_{k,k_1}/(\omega - \omega_{\alpha,k})$. One can then use the Langreth rules together with Eq. (14), to find the “lesser” SE defined in Eq. (5) of the main text.

Cavity photons Green’s functions

Let us now show that the time-ordered photon GF $D(\omega)$ satisfies the Dyson equation given in the main text. We start by taking the second time derivative of the cavity vector potential $A(t)$, and then use the Heisenberg equation $\partial_\tau A(\tau) = i[H, A](\tau)$ two times. As in the previous section, we consider a vanishing source term $H' = \mathcal{J}A$ in the Hamiltonian H . Then, we take the functional derivative of the ground-state expectation of the obtained equation with respect to $\mathcal{J}(t')$. This calculation yields the following equation of motion for $D(\omega)$:

$$\left(-\frac{\partial_\tau^2}{2\omega_0} - \frac{\omega_0}{2}\right) D(\tau - \tau') = \delta(\tau - \tau') - ig \sum_{\alpha,\alpha'} \sum_k (1 - \delta_{\alpha,\alpha'}) \delta_{\mathcal{J}(\tau')} G_{\alpha,k,\alpha',k}(\tau, \tau^+) + \sum_{\mathbf{p}} \mu_{\mathbf{p}} D_{\mathbf{p}}(\tau - \tau'), \quad (22)$$

where the time τ^+ is τ plus a positive vanishing quantity, and $D_{\mathbf{p}}(\tau - \tau') = -i\langle \mathcal{T} A_{\mathbf{p}}(\tau) A(\tau') \rangle$ describes the correlations between the cavity mode and the electromagnetic environment. The equation of motion satisfied by $D_{\mathbf{p}}$ can be derived similarly as before (by taking its second time derivative), namely:

$$(-\partial_\tau^2 - \omega_{\mathbf{p}}^2) D_{\mathbf{p}}(\tau - \tau') = 2\omega_{\mathbf{p}} \mu_{\mathbf{p}} D(\tau - \tau'), \quad (23)$$

which is formally solved in the frequency domain as $D_{\mathbf{p}}(\omega) = \mu_{\mathbf{p}} \mathcal{D}_{\mathbf{p}}(\omega) D(\omega)$. Here, $\mathcal{D}_{\mathbf{p}}(\omega) = -i \int d(\tau - \tau') e^{i\omega(\tau - \tau')} \langle \mathcal{T} A_{\mathbf{p}}(\tau) A_{-\mathbf{p}}(\tau') \rangle_0 = 2\omega_{\mathbf{p}}/(\omega^2 - \omega_{\mathbf{p}}^2)$ denotes the extra-cavity photon GF. On the other hand, the second term in the right-hand side of Eq. (22) can be calculated in a similar fashion as in Sec. , namely:

$$\delta_{\mathcal{J}(\tau')} G_{\alpha,k,\alpha',k}(\tau, \tau^+) = g \sum_{k_1,k_2} \int d\tau_1 \int d\tau_2 \int d\tau_3 G_{\alpha,k,k_1}(\tau - \tau_1) \Lambda_{\alpha,k_1,\alpha',k_2}(\tau_1, \tau_2, \tau_3) D(\tau_3 - \tau') G_{\alpha',k_2,k}(\tau_2 - \tau^+), \quad (24)$$

where the vertex function is defined in Eq. (19). In the FBA, we assume $\Lambda_{\alpha,k_1,\alpha',k_2}(\tau_1, \tau_2, \tau_3) = (1 - \delta_{\alpha,\alpha'}) \delta_{k_1,k_2} \delta(\tau_1 - \tau_2) \delta(\tau_1 - \tau_3)$, which inserted in Eq. (24), allows us to write the equation of motion (22) in the Dyson form $(D_0^{-1}(\omega) - \Pi(\omega)) D(\omega) = 1$, with the bare photon GF $D_0(\omega) = 2\omega_0/(\omega^2 - \omega_0^2)$, and the photon SE:

$$\Pi(\omega) = -ig^2 \sum_{\alpha,\alpha'} \sum_{k,k_1} (1 - \delta_{\alpha,\alpha'}) \int \frac{d\omega'}{2\pi} G_{\alpha,k,k_1}(\omega + \omega') G_{\alpha',k_1,k}(\omega') + \sum_{\mathbf{p}} \mu_{\mathbf{p}}^2 \mathcal{D}_{\mathbf{p}}(\omega). \quad (25)$$

The summation over \mathbf{p} is then converted into a frequency integral, $\sum_{\mathbf{p}} \rightarrow \int_0^\infty d\omega \rho_0(\omega)$, where $\rho_0(\omega)$ denotes the extra-cavity photon density of states. Introducing the cavity photon decay rate as $\kappa(\omega) = 2\pi\rho_0(\omega)\mu^2(\omega)$ (assumed to be frequency-independent, $\kappa(\omega) \equiv \kappa$), using the Langreth rules and the result $\mathcal{D}_{\mathbf{p}}^>(\omega) = -2i\pi\delta(\omega - \omega_{\mathbf{p}})$, we can conclude that the “greater” photon SE coincides with the expression given by Eq. (6) in the main text.

Note that the photon GF $D^<(\omega)$ can be used to compute the mean photon number in the steady state (up to small squeezing terms) as $N_{\text{ph}} = -\frac{1}{2} \left(\int \frac{d\omega}{2\pi} \Im D^<(\omega) + 1 \right)$. We have checked that these photon numbers remain always small, reaching at most $N_{\text{ph}} \sim 10^{-2}$, which shows that our system is in a purely quantum regime regarding the electro-magnetic field in the cavity.

Self-consistent procedure

In the previous sections, we have shown that electron/photon SEs and GFs are related to each other by a self-consistent, closed set of integro-differential equations. The numerical procedure to solve these equations self-consistently is as follow: we start with the electron SEs $\underline{\Sigma}_\alpha^{\leq}$ defined in Eq. (5) of the main text (it is easy to show that $\underline{\Sigma}_\alpha^>$ satisfies a similar equation). The first order is obtained by replacing the fully interacting GFs $\underline{G}_\alpha^{\leq}$ and D^{\leq} by the non-interacting ones $\underline{G}_\alpha^{0\leq}$ and D_0^{\leq} , evaluated in the ground state of H_0 :

$$G_{\alpha,k,k'}^{0<}(\omega) = 2i\pi n_{\alpha,k} \delta_{k,k'} \delta(\omega - \omega_{\alpha,k}), \quad G_{\alpha,k,k'}^{0>}(\omega) = -2i\pi(1 - n_{\alpha,k}) \delta_{k,k'} \delta(\omega - \omega_{\alpha,k}), \quad (26)$$

and $D_0^<(\omega) = -2i\pi\delta(\omega + \omega_0)$, $D_0^>(\omega) = -2i\pi\delta(\omega - \omega_0)$. The retarded and advanced SEs can then be efficiently calculated using the real-time equality[70] $\underline{\Sigma}_\alpha^r(t) = \theta(t) (\underline{\Sigma}_\alpha^>(t) - \underline{\Sigma}_\alpha^<(t))$. Introducing the real function $\underline{\chi}_\alpha(\omega) = i(\underline{\Sigma}_\alpha^>(\omega) - \underline{\Sigma}_\alpha^<(\omega))$, the previous equality can be written in the frequency domain as:

$$\underline{\Sigma}_\alpha^r(\omega) = -i \frac{\underline{\chi}_\alpha(\omega)}{2} + \frac{1}{2\pi} \text{p.v} \int d\omega' \frac{\underline{\chi}_\alpha(\omega')}{\omega - \omega'}, \quad (27)$$

where p.v denotes the Cauchy principal value. As a causal function, the real and imaginary parts of $\underline{\Sigma}_\alpha^r(\omega)$ are related to each other by Kramers-Kronig relations, as it can be checked directly from Eq. (27). The advanced SE is simply given by $\underline{\Sigma}_\alpha^a(\omega) = (\underline{\Sigma}_\alpha^r(\omega))^\dagger$. The function $\underline{\chi}_\alpha(\omega)$ is related to the Bloch states spectral broadening induced by the coupling to the leads and the cavity mode, while the real part of $\underline{\Sigma}_\alpha^r(\omega)$ provides a shift of the Bloch state energies $\omega_{\alpha,k}$. Plugging these results in the Dyson and Keldysh equations given in the main text, we calculate the first-order electron GFs $\underline{G}_\alpha^\beta$ ($\beta = r, a$) and $\underline{G}_\alpha^{\leq}$, and use the latter to compute the first-order photon SEs Π^{\leq} defined in Eq. (6) of the main text. The retarded and advanced parts Π^β are obtained using the relation $\Pi^r(t) = \theta(t) (\Pi^>(t) - \Pi^<(t))$, and can be inserted into the Dyson and Keldysh equations to calculate the first-order photon GFs D^β and D^{\leq} . Finally, the second-order electron SE is obtained from Eq. (5) of the main text, with the first-order electron and photon GFs, and the whole cycle is then repeated until convergence. Namely, this procedure is repeated a sufficient number of times, such that the total current flowing through the bands has converged. where p.v denotes the Cauchy principal value. As a causal function, the real and imaginary parts of $\underline{\Sigma}_\alpha^r(\omega)$ are related to each other by Kramers-Kronig relations, as it can be checked directly from Eq.(27). The advanced SE is simply given by $\underline{\Sigma}_\alpha^a(\omega) = (\underline{\Sigma}_\alpha^r(\omega))^\dagger$. The function $\underline{\chi}_\alpha(\omega)$ is related to the Bloch states spectral broadening induced by the coupling to the leads and the cavity mode, while the real part of $\underline{\Sigma}_\alpha^r(\omega)$ provides a shift of the Bloch state energies $\omega_{\alpha,k}$. Plugging these results in the Dyson and Keldysh equations given in the main text, we calculate the first-order electron GFs $\underline{G}_\alpha^\beta$ ($\beta = r, a$) and $\underline{G}_\alpha^{\leq}$, and use the latter to compute the first-order photon SEs Π^{\leq} defined in Eq. (6). The retarded and advanced parts Π^β are obtained using the relation $\Pi^r(t) = \theta(t) (\Pi^>(t) - \Pi^<(t))$, and can be inserted into the Dyson and Keldysh equations to calculate the first-order photon GFs D^β and D^{\leq} . Finally, the second-order electron SE is obtained from Eq. (5) of the main text, with the first-order electron and photon GFs, and the whole cycle is then repeated until convergence. Namely, this procedure is repeated a sufficient number of times, such that the total current flowing through the bands has converged.

Second order spectral broadening

The scaling of the electron spectral broadening induced by the light-matter coupling can be found by evaluating analytically the second-order ($\propto g^2$) electron SE. The latter is obtained by replacing the fully interacting GFs $\underline{G}_\alpha^{\leq}$ and

D_0^{\lessgtr} in Eq. (5) of the main text by the non-interacting ones $G_\alpha^{0\lessgtr}$ and D_0^{\lessgtr} . Considering the resonant case $\omega_{21} = \omega_0 = 1$, the second-order broadening defined in Sec. is calculated as:

$$\chi_{\alpha,k,k'}(\omega) = \frac{4\kappa g^2 (1 - \delta_{\alpha,\alpha'}) \delta_{k,k'}}{((\omega - \omega_{\alpha',k})^2 - 1)^2 + 4\kappa^2} \left((1 - n_{\alpha',k}^0) \theta(\omega - \omega_{\alpha',k}) + n_{\alpha',k}^0 \theta(\omega_{\alpha',k} - \omega) \right) + \Gamma (\sigma_{k,k'}^N - \sigma_{k,k'}^1), \quad (28)$$

where $n_{\alpha',k}^0$ represents the Fermi occupation number of the Bloch state k in the band α' , for $g = 0$. Letting the leads contribution aside [second term in the right-hand side of Eq. (28)], the broadening is diagonal with respect to k . Considering a Bloch state k in the lowest band $\alpha = 1$, its light-induced broadening depends on the filling of the state k in the upper band $\alpha' = 2$. When $n_{2,k} = 1$, the associated electron can undergo a transition from the upper to the lower band by emitting a photon with energy $\omega_0 = 1$. This yields a broadening $\propto g^2/\kappa$ in the vicinity of $\omega = \omega_{2,k} - 1 \approx \omega_1$.

Comparison with a quantum master equation model

It is interesting to compare the results obtained using NEGFs with a method based on the exact numerical solving of the quantum master equation (up to a certain photon number considered as a cutoff in the system's Hilbert space). In this case, the effect of the (Markovian) environment is cast in terms of dissipators, providing both the decay of cavity photons with rate κ , as well as the injection/extraction of electrons in the chain with rate Γ . The corresponding quantum master equation reads $\partial_t \hat{\rho} = -i[H_S, \hat{\rho}] + \mathcal{L}\hat{\rho}$, where

$$\mathcal{L}\hat{\rho} = \frac{\kappa}{2} \mathcal{D}[a]\hat{\rho} + \frac{\Gamma}{2} \sum_{\alpha=1}^2 \left(\mathcal{D}[c_{\alpha,1}^\dagger]\hat{\rho} + \mathcal{D}[c_{\alpha,N}]\hat{\rho} \right) \quad (29)$$

determines the time evolution of the system density operator $\hat{\rho}$, with the Lindblad terms:

$$\mathcal{D}[b]\hat{\rho} = -\{b^\dagger b, \hat{\rho}\} + 2b\hat{\rho}b^\dagger. \quad (30)$$

In the steady state, $\partial_t \hat{\rho} = 0$, and the current can be written as:

$$J = \frac{e\Gamma}{2} \sum_{\alpha} \text{Tr} \left[c_{\alpha,1}^\dagger c_{\alpha,1} \{ \mathcal{D}[c_{\alpha,1}^\dagger] \hat{\rho} \} \right], \quad (31)$$

where Tr denotes the trace on the system Hilbert space. Due to the exponential scaling of the Hilbert space size with the chain length, this method can be only applied for small systems ($N \sim 5$).

On Fig. 5, we have represented a comparison between the results obtained with the NEGF and the quantum master equation approaches (QME). The steady-state current $J/(e\Gamma)$ is represented as a function of g in the collective dressing regime with $N = 3$, $\Gamma = 2.5 \times 10^{-4}$, $t = 2.5 \times 10^{-3}$, $\kappa = 0.05$ [panel (a)], and in the individual dressing regime with $N = 3$, $\Gamma = 2.5 \times 10^{-4}$, $t = 0.07$, $\kappa = 0.005$ [panel (b)]. The absolute difference $\Delta J/(e\Gamma)$ between the two methods is represented in the bottom panels, in (c) the collective dressing regime and (d) the individual dressing regime. The validity of the NEGF model depends on the smallness of the perturbative parameter $g^2/(4t\kappa)$. As expected, the absolute difference between the results obtained by the two methods scales as g^2 for small g . By evaluating the perturbative parameter $g^2/(4t\kappa)$ when g is on the high side in the considered range, one realizes that it is actually close to unity for $g \sim 0.03$, which explains the rather large discrepancy ($\Delta J \sim 0.1e\Gamma$) between the two methods in this range. However, the qualitative trends are unchanged, and the NEGF model is still expected to give a correct physical description of the system, even close to the boundaries of this perturbative approach.

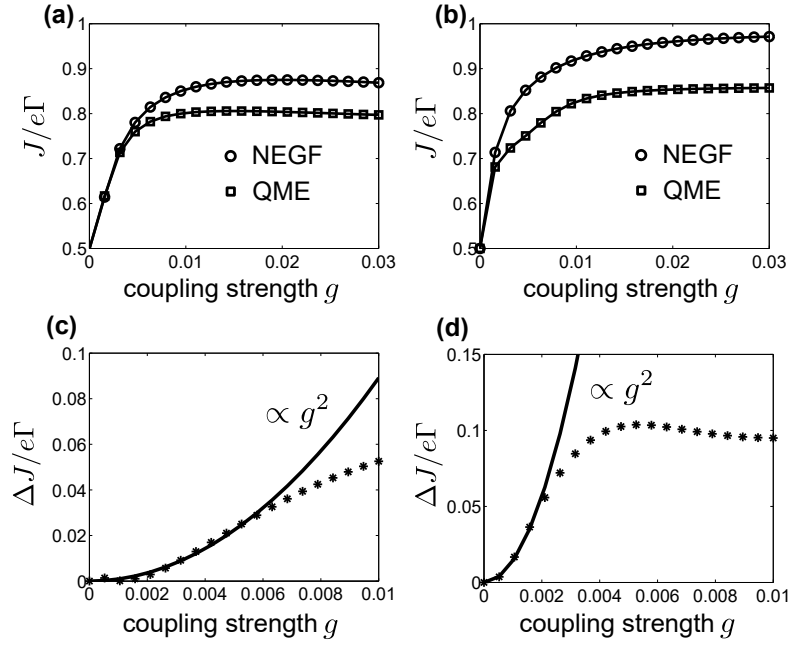


FIG. 5. Comparison between the results obtained with the NEGF and the quantum master equation approach (QME). Top panels: Steady-state current $J/(e\Gamma)$ as a function of g in (a) the collective dressing regime with $N = 3$, $\Gamma = 2.5 \times 10^{-4}$, $t = 2.5 \times 10^{-3}$, $\kappa = 0.05$, (b) the individual dressing regime with $N = 3$, $\Gamma = 2.5 \times 10^{-4}$, $t = 0.07$, $\kappa = 0.005$. Bottom panels: Absolute difference $\Delta J/(e\Gamma)$ between the two methods as a function of g , in (c) the collective dressing regime, (d) the individual dressing regime.